10

Tests and Probes of Big Bang Cosmology

In this final chapter, we review three experimental predictions of the cosmological model that we developed in chapter 9, and their observational verification. The tests are cosmological redshift (in the context of distances to type-Ia supernovae, and baryon acoustic oscillations), the cosmic microwave background, and nucleosynthesis of the light elements. Each of these tests also provides information on the particular parameters that describe our Universe. We conclude with a brief discussion on the use of quasars and other distant objects as cosmological probes.

10.1 Cosmological Redshift and Hubble's Law

Consider light from a galaxy at a comoving radial coordinate r_e . Two wavefronts, emitted at times t_e and $t_e + \Delta t_e$, arrive at Earth at times t_0 and $t_0 + \Delta t_0$, respectively. As already noted in chapter 4.5 in the context of black holes, the metric of spacetime dictates the trajectories of particles and radiation. Light, in particular, follows a null geodesic with ds = 0. Thus, for a photon propagating in the FLRW metric (see also chapter 9, Problems 1–3), we can write

$$0 = c^2 dt^2 - R(t)^2 \frac{dr^2}{1 - kr^2}. (10.1)$$

The first wavefront therefore obeys

$$\int_{t_e}^{t_0} \frac{dt}{R(t)} = \frac{1}{c} \int_0^{r_e} \frac{dr}{\sqrt{1 - kr^2}},$$
(10.2)

and the second wavefront

$$\int_{t_e + \Delta t_e}^{t_0 + \Delta t_0} \frac{dt}{R(t)} = \frac{1}{c} \int_0^{r_e} \frac{dr}{\sqrt{1 - kr^2}}.$$
(10.3)

© Copyright, Princeton University Press. No part of this book may be distributed, posted, or reproduced in any form by digital or mechanical means without prior written permission of the publisher.

248 | Chapter 10

Since r_e is comoving, the right-hand sides of both equalities are independent of time, and therefore equal. Equating the two left-hand sides, we find

$$\int_{t_{c}+\Delta t_{c}}^{t_{0}+\Delta t_{0}} \frac{dt}{R(t)} - \int_{t_{c}}^{t_{0}} \frac{dt}{R(t)} = 0.$$
 (10.4)

Expressing the first integral as the sum and difference of three integrals, we can write

$$\int_{t_e}^{t_0} - \int_{t_e}^{t_e + \Delta t_e} + \int_{t_0}^{t_0 + \Delta t_0} - \int_{t_e}^{t_0} = 0,$$
(10.5)

and the first and fourth terms cancel out. Since the time interval between emission of consecutive wavefronts, as well as the interval between their reception, is very short compared to the dynamical timescale of the Universe ($\sim 10^{-15}$ s for visual light, vs. $\sim 10^{17}$ s for a Hubble time), we can assume that R(t) is constant between the two emission events and between the two reception events. We can then safely approximate the integrals with products:

$$\frac{\Delta t_e}{R(t_e)} = \frac{\Delta t_0}{R(t_0)}. (10.6)$$

Recalling that

$$\Delta t_e = \frac{1}{\nu_e} = \frac{\lambda_e}{c} \tag{10.7}$$

and

$$\Delta t_0 = \frac{1}{v_0} = \frac{\lambda_0}{c},\tag{10.8}$$

we find that

$$\frac{\Delta t_0}{\Delta t_e} = \frac{\lambda_0}{\lambda_e} = \frac{\nu_e}{\nu_0} = \frac{R(t_0)}{R(t_e)} \equiv 1 + z,$$
 (10.9)

where we have defined the **cosmological redshift**, *z*. Thus, the further in the past that the light we receive was emitted (i.e., the more distant a source), the more the light is redshifted, in proportion to the ratio of the scale factors today and then. This, therefore, is the origin of Hubble's law.

Just like Doppler shift, the cosmological redshift of a distant object can be found easily by obtaining its spectrum and measuring the wavelengths of individual spectral features, either in absorption or in emission, relative to their laboratory wavelengths. Note, however, that cosmological redshift is distinct from Doppler, transverse-Doppler, and gravitational redshifts. The cosmological redshift of objects that are comoving with the Hubble flow is the result of the expansion of the scale of the Universe that takes place between emission and reception of a signal. In an expanding Universe (such as ours), $R(t_0) > R(t_e)$ always, and therefore z is always a redshift (rather than a blueshift). Indeed, it is found observationally that, beyond a distance of about 20 Mpc, all sources of light, without exception,

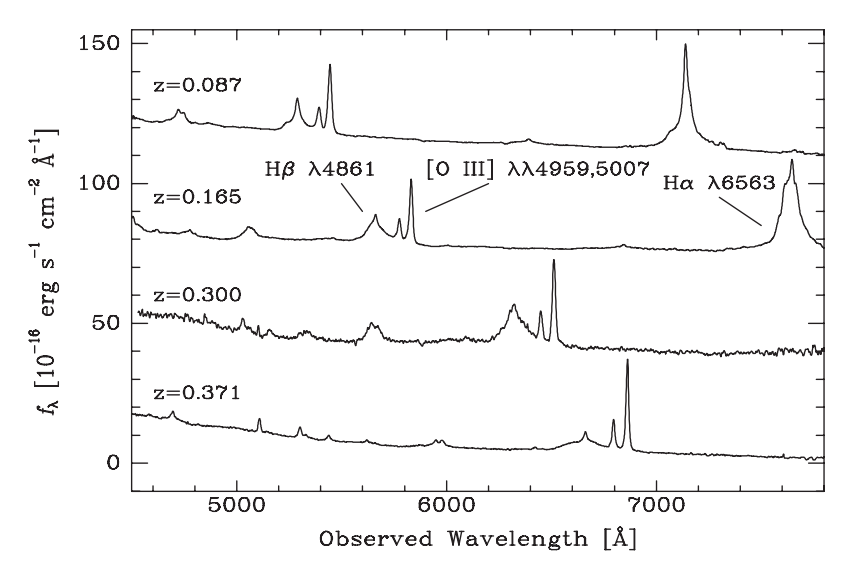


Figure 10.1 Optical spectra of four quasars, with cosmological redshifts increasing from top to bottom, as marked. Note the progression to the red of the main emission lines, which are indicated. The width of the Balmer lines is the result of Doppler blueshifts and redshifts about the line centers, due to internal motions of the emitting gas, under the influence of the central black holes powering the quasars. The [O III] lines are narrower because they are emitted by gas with smaller internal velocities. Data credit: S. Kaspi et al. 2000, *Astrophys. J.*, 533, 631.

are redshifted.¹ In addition to the cosmological redshift, the spectra of distant objects can be affected by (generally smaller) redshifts or blueshifts due to the other effects. Figure 10.1 shows the spectra of several distant quasars (objects that were discussed in chapter 7.3). Note the various redshifts by which the emission lines of each quasar (hydrogen Balmer H α and H β , and the doublet [O III] $\lambda\lambda$ 4959, 5007 are the most prominent) have been shifted from their rest wavelengths by the cosmological expansion.

We have seen that the evolution of the scale factor, R(t), depends on the parameters that describe the Universe: H_0 , k, Ω_m , and Ω_Λ . This suggests that, if we could measure R(t) at different times in the history of the Universe, we could deduce what kind of a universe we live in. In practice, it is impossible to measure R(t) directly. However, the cosmological redshift z of an object gives the ratio between the scale factors today and at the time the light was emitted. We can therefore deduce the cosmological parameters by measuring properties of distant objects that depend on R(t) through the redshift. Two such

¹ Nearby objects, such as Local Group galaxies and the stars in the Milky Way, are not receding with the Hubble flow (nor will they in the future) because they are bound to each other and to us. Similarly, the stars themselves, the Solar System, the Earth, and our bodies do not expand as the Universe grows. There is a long and unresolved debate as to what is the true nature of the observed expansion. One interpretation is that the cosmological expansion arises from the "stretching of space itself," and that the static galaxies are swept along with this stretching "fabric." An opposing view is that an expanding space is not a physically meaningful concept. Rather, galaxies are receding from us simply because they were doing so in the past, i.e., they have initial recession velocities and inertia (although now they are aided by dark energy—see below). In this view, the observed redshifts are essentially kinematic Doppler shifts. In both views (although for different reasons), a test particle placed at rest at any distance from us would not join the Hubble flow.

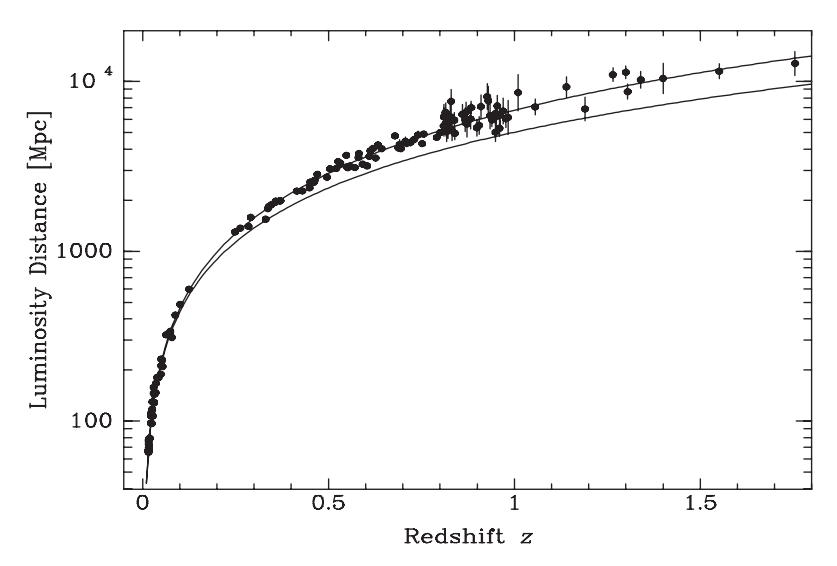


Figure 10.2 A Hubble diagram extending out to redshift $z\approx 1.7$, based on type-Ia supernovae. Note that redshift now replaces velocity (compare to Fig. 8.6) and the *luminosity distances* to these standard candles are now plotted on the vertical axis. The top and bottom curves give the expected relations for cosmologies with $\Omega_m=0.3$, $\Omega_\Lambda=0.7$, and $\Omega_m=1$, $\Omega_\Lambda=0$, respectively. The data favor the top curve, indicating a cosmology currently dominated by dark energy. The calculation of the curves is outlined in Problems 4–7. Data credits: A. Riess et al. 2004, *Astrophys. J.*, 607, 665, and P. Astier et al. 2006, *Astron. Astrophys.*, 447, 31.

properties that have been particularly useful are the flux from an object and its angular size. Models with different cosmological parameters make different predictions as to how these observables change as a function of redshift. Measuring the flux from a "standard candle" to derive a "distance," and plotting the distance vs. the "velocity," is, of course, the whole idea behind the Hubble diagram. Now, however, we realize that cosmological redshift is distinct from Doppler velocity. Furthermore, in a curved and expanding space, "distance" can be defined in a number of different ways, and will depend on the properties and history of that space. Nevertheless, observables (e.g., the flux from an object of a given luminosity, or the angular size of an object of a given physical size, at some redshift) can be calculated straightforwardly from the FLRW metric and the Friedmann equations and compared to the observations. We will work out examples of such calculations in section 10.3, and in Problems 4–7 at the end of this chapter.

In recent years, the Hubble diagram, based on type-Ia supernovae serving as standard candles, has been measured out to a redshift z=2, corresponding to a time when the Universe was about a quarter its present age. Figure 10.2 shows an example. The intrinsic luminosity of the supernovae at maximum light, compared to their observed flux, permits us to define a cosmological distance called **luminosity distance**:

$$D_L \equiv \left(\frac{L}{4\pi f}\right)^{1/2}.\tag{10.10}$$

The observed supernova fluxes (or, equivalently, their luminosity distances) vs. redshift are best reproduced by a model in which the Universe is currently in an accelerating stage, into which it transited (from the initial deceleration) at a time corresponding to about $z \sim 1$. If one assumes a flat, k=0 Universe (for which the evidence will be presented in section 10.3), the data indicate $\Omega_m \approx 0.3$ and $\Omega_\Lambda \approx 0.7$. If this is true, the dynamics of the Universe are currently dominated by a "dark energy" of unknown source and nature that is causing the expansion to accelerate. The cosmological constant case, treated in chapter 9.5, is one possible form of the dark energy.

In the derivation of cosmological redshift, above, we considered the propagation of individual wavefronts of light. Instead, we could have discussed the propagation of, say, individual photons, or brief light flashes, but would have gotten the same result: the time interval between emission of consecutive photons or light signals appears lengthened to the observer by a factor 1+z. Thus, in addition to cosmological redshift, light signals will undergo **cosmological time dilation**. For example, if a source at redshift z is emitting photons at a certain wavelength and at some rate, not only will an observer see the wavelength of every photon increased by 1+z, but the photon arrival rate will also be lower by 1+z. Both of these effects will reduce the observed energy flux, in addition to the reduction due to geometrical $(4\pi \times \text{distance}^2)$ dilution (see Problem 3).

10.2 The Cosmic Microwave Background

Since the mean density of the Universe increases monotonically as one goes back in time,² there must have been an early time when the density was high enough such that the mean free path of photons was small, and baryonic matter and radiation were in thermodynamic equilibrium. The radiation field then had a Planck spectrum. Since the energy density of radiation changes with the scale factor as (Eq. 9.40)

$$\rho \propto R^{-4},\tag{10.11}$$

but this energy density also relates to a temperature as

$$\rho = aT^4, \tag{10.12}$$

we can consider a temperature of the Universe at this stage, which varied as

$$T \propto \frac{1}{R}.\tag{10.13}$$

Therefore, early enough, the Universe was not only dense but also hot. At some stage, the temperature must have been high enough such that all atoms were constantly being ionized. The main source of opacity was then electron scattering. Going forward in time

 $^{^2}$ In principle, models with a large enough positive cosmological constant permit a currently expanding Universe that had, in its past, a minimum R that is greater than zero, and thus no initial singularity. At times before the minimum, the Universe would have been contracting. In such a universe, as one looks to larger and larger distances, objects at first have increasing redshifts, as usual. However, beyond some distance, objects begin having progressively smaller redshifts, and eventually blueshifts. Such a behavior is contrary to observations.

now, the temperature declined, and at $T \sim 3000$ K, few of the photons in the radiation field, even in its high-energy tail, had the energy required to ionize a hydrogen atom. Most of the electrons and protons then recombined. Once this happened, at a time $t_{\rm rec} = 380,000$ yr after the Big Bang, the major source of opacity disappeared, and the Universe became transparent to radiation of most frequencies.³ As we look to large distances in any direction in the sky, we look back in time, and therefore at some point our sight line must reach the **surface of last scattering**, beyond which the Universe is opaque.

The photons emerging from the last-scattering surface undergo negligible additional scattering and absorption until they reach us. Their number density therefore decreases, as the Universe expands, inversely with the volume, as R^{-3} . In addition, the energy of every photon is reduced by R^{-1} due to the cosmological redshift. The photon *energy* density therefore continues to decline as R^{-4} . Furthermore, the spectrum keeps its Planck shape, even though the photons are no longer in equilibrium with matter. To see this, consider that every photon gets redshifted from its emitted frequency ν to an observed frequency ν' according to the transformation

$$v' = \frac{v}{1+z}, \quad dv' = \frac{dv}{1+z}.$$
 (10.14)

Next, recall the form of the Planck spectrum,

$$B_{\nu} = \frac{2h\nu^3}{c^2} \frac{d\nu}{e^{h\nu/kT} - 1}.$$
 (10.15)

Dividing by the energy of a photon, $h\nu$, we obtain the *number* density of photons per unit frequency interval,

$$n_{\nu} = \frac{2\nu^2}{c^2} \frac{d\nu}{e^{h\nu/kT} - 1}.$$
 (10.16)

Since the number of photons is conserved, their density decreases by a factor $(1 + z)^3$, and the new distribution will be

$$n'_{\nu'} = \frac{n_{\nu}}{(1+z)^3} = \frac{2\nu^2}{c^2} \frac{d\nu}{e^{h\nu/kT} - 1} \frac{1}{(1+z)^3} = \frac{2\nu'^2}{c^2} \frac{d\nu'}{e^{h\nu'/kT'} - 1},$$
(10.17)

where

$$T' \equiv \frac{T}{1+z}. ag{10.18}$$

In other words, the spectrum keeps the Planck form, but with a temperature that is reduced, between the time of recombination and the present, according to

$$T_{\rm cmb} = \frac{T_{\rm rec}}{1 + z_{\rm rec}},\tag{10.19}$$

where z_{rec} is the redshift at which recombination occurs. A prediction of Big Bang cosmology is therefore that space today should be filled with a thermal photon distribution arriving from all directions in the sky.

³ The ubiquitous presence of hydrogen atoms in their ground state made the Universe, at this point, very opaque to ultraviolet radiation with wavelengths shortward of Lyman- α .

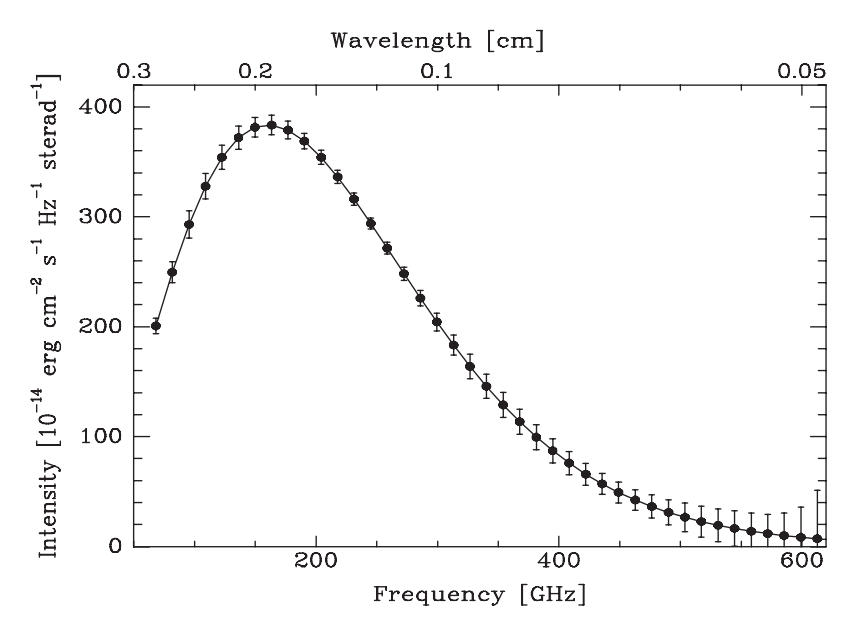


Figure 10.3 Observed spectrum of the cosmic microwave background, compared with a T = 2.725-K blackbody curve. The error bars shown are 500σ , so as to be discernible in the plot. Data credit: D. J. Fixsen et al. 1996, Astrophys. J., 473, 576.

In the 1940s Gamow predicted, based on considerations of nucleosynthesis (which are discussed in the next section) that recombination must have occurred at $z_{\rm rec}\sim 1000$, and hence the thermal spectrum should correspond to a temperature of a few to a few tens of degrees Kelvin (i.e., with a peak at a wavelength of order 1 mm, in the microwave region of the spectrum). This cosmic microwave background (CMB) radiation was discovered accidentally in 1965 by Penzias and Wilson, while studying sources of noise in microwave satellite communications. They translated the intensity they measured at a single frequency into a temperature, $T_{\rm cmb} \approx 3$ K, by assuming that the radiation has a Planck spectrum and that the frequency is on the Rayleigh–Jeans side of the distribution⁴ (Eq. 2.18), according to

$$B_{\nu} \approx \frac{2\nu^2}{c^2}kT. \tag{10.20}$$

Subsequent measurements, especially with several recent space-based experiments, have confirmed that the spectrum has a precise blackbody form, and have refined the temperature measurement to $T_{\rm cmb} = 2.725 \pm 0.002$ K (see Fig. 10.3). Note that the CMB solves the Olbers paradox in a surprising way: every line of sight does indeed reach an ionized surface with a temperature similar to that of the photosphere of a star. Despite our being inside such an oven, we are not grilled because the expansion of the Universe dilutes the radiation emitted by this surface, and shifts it to harmless microwave energies.

⁴ As opposed to the thermal flux from a star of unknown surface area, for which a temperature cannot be deduced from one or more measurements solely on the Rayleigh-Jeans side, the CMB is an intensity, i.e., an energy flux per unit solid angle on the sky, and it is completely specified for a blackbody of a given temperature. A temperature derived in this way is called by radio astronomers a brightness temperature.

© Copyright, Princeton University Press. No part of this book may be distributed, posted, or reproduced in any form by digital or mechanical means without prior written permission of the publisher.

254 | Chapter 10

The photon number density due to the CMB is

$$n_{\gamma,\text{cmb}} \sim \frac{aT^4}{2.8kT} = \frac{7.6 \times 10^{-15} \text{ cgs} \times (2.7 \text{ K})^3}{2.8 \times 1.4 \times 10^{-16} \text{ erg K}^{-1}} = 400 \text{ cm}^{-3}.$$
 (10.21)

Let us see that this is much larger than the cosmic mean number density of photons originating from stars. If $n_{\rm gal}$ is the mean number density of L_* galaxies, then at a typical point in the Universe the flux of starlight from galaxies within a spherical shell of thickness dr at a distance r from this point is

$$df = \frac{L_* n_{\rm gal} 4\pi r^2 dr}{4\pi r^2} = L_* n_{\rm gal} dr. \tag{10.22}$$

For a rough, order-of-magnitude estimate of the total flux from galaxies at all distances, let us ignore the Universal expansion, possible curvature of space, and evolution with time of L_* and $n_{\rm gal}$, and integrate from r=0 to $r=ct_0$, where t_0 is the age of the Universe. Then the total flux is $f=L_*n_{\rm gal}ct_0$. Stars produce radiation mostly in the optical/IR range, with photon energies of order $h\nu_{\rm opt}\sim 1$ eV. The stellar photon density is about 1/c times the photon flux. Thus,

$$\begin{split} n_{\gamma,*} &\sim \frac{L_* n_{\rm gal} t_0}{h \nu_{\rm opt}} \approx \frac{10^{10} L_{\odot} \times 10^{-2} \text{ Mpc}^{-3} \times 14 \text{ Gyr}}{1 \text{ eV}} \\ &= \frac{10^{10} \times 3.8 \times 10^{33} \text{ erg s}^{-1} \times 10^{-2} \times (3.1 \times 10^{24} \text{ cm})^{-3} \times 4.4 \times 10^{17} \text{ s}}{1.6 \times 10^{-12} \text{ erg}} \\ &\approx 4 \times 10^{-3} \text{ cm}^{-3}. \end{split}$$
(10.23)

Thus, there are of order 10⁵ CMB photons for every stellar photon.⁵

The present-day baryon mass density is about 4% of the critical closure density, ρ_c . The mean baryon *number* density is therefore

$$n_B \approx \frac{0.04 \rho_c}{m_p} \approx \frac{0.04 \times 9.2 \times 10^{-30} \text{ g cm}^{-3}}{1.7 \times 10^{-24} \text{ g}} = 2 \times 10^{-7} \text{ cm}^{-3}.$$
 (10.24)

(Less than one-tenth of these baryons are in stars, and the rest are in a very tenuous intergalactic gas.) The baryon-to-photon ratio is therefore

$$\eta \equiv \frac{n_{\rm B}}{n_{\nu}} \approx 5 \times 10^{-10}.\tag{10.25}$$

Thus, although the *energy* density due to matter is much larger than that due to radiation (Eqs. 9.65 and 9.66), the *number* density of photons is much larger than the mean number density of baryons.

 $^{^5}$ The mean stellar photon density above is, of course, not representative of the stellar photon density on Earth, which is located inside an L_* galaxy, very close to an L_{\odot} star. The daylight solar photon density on Earth (see Eq. 3.8) is 10^{10} times greater than the mean stellar value for the Universe, found above, and is thus also much greater than the CMB photon density.

10.3 Anisotropy of the Microwave Background

The temperature of the CMB, T=2.725 K, is extremely uniform across the sky. There is a small **dipole** in the CMB sky, arising from the Doppler effect due mostly to the motion of the Local Group (at a velocity of \approx 600 km s⁻¹) relative to the comoving cosmological frame. Apart from the dipole, the only deviations from uniformity in the CMB sky are temperature **anisotropies**, i.e., regions of various angular sizes with temperatures different from the mean, with fluctuations having root-mean-squared $\delta T=29~\mu\text{K}$, or

$$\frac{\delta T}{T} \sim 10^{-5}$$
. (10.26)

Figure 10.4 shows a map of these temperature fluctuations. The extreme isotropy of the appearance of the Universe at $z\sim 1000$ is an overwhelming justification of the assumption of homogeneity and isotropy inherent to the cosmological principle. However, this extreme isotropy raises the questions of *why* and *how* the Universe can appear so isotropic. At the time of recombination, the horizon size—the size of a region in space across which light can propagate since the Big Bang (see chapter 9, Problems 1–3)—corresponded to a physical region that subtends only about 2° on the sky today. Thus, different regions separated by more than $\sim 2^{\circ}$ could not have been in causal contact by $t_{\rm rec}$, and therefore it is surprising that they would have the same temperature to within 10^{-5} . CMB photons from opposite directions on the sky have presumably never been in causal contact until now, yet they have almost exactly the same temperature.

The currently favored explanation for this "horizon problem" is that, very early during the evolution of the Universe, in the first small fraction of a second, there was an epoch of **inflation**. During that epoch, a vacuum energy density with negative pressure caused an exponential expansion of the scale factor, much like the second acceleration epoch that, apparently, we are in today. The inflationary expansion led causally connected regions to expand beyond the size of the horizon at that time. All the different parts of the microwave sky we see today were, in fact, part of a small, causally connected region before inflation. The cause and details of inflation are still a matter of debate, but most versions of the theory predict that, today, space is almost exactly flat (i.e., $\Omega_m + \Omega_\Lambda$ is very close to 1). We will see now that this prediction is strongly confirmed by the observed characteristics of the anisotropies.

The temperature anisotropies in the CMB arise through a number of processes, but at their root are small-amplitude inhomogeneities in the nearly uniform cosmic mass distribution. These inhomogeneities are set up at the end of the inflationary era, and their characteristics are yet another prediction of inflation theories. Most of the mass density at that time, as now, is in a nonbaryonic, pressureless, dark matter. Mixed with the dark matter, and sharing the same inhomogeneity pattern, is a relativistic gas of baryons and radiation. The photon–baryon gas therefore has an equation of state that is well described by

$$P = \frac{1}{3}\rho c^2. {(10.27)}$$

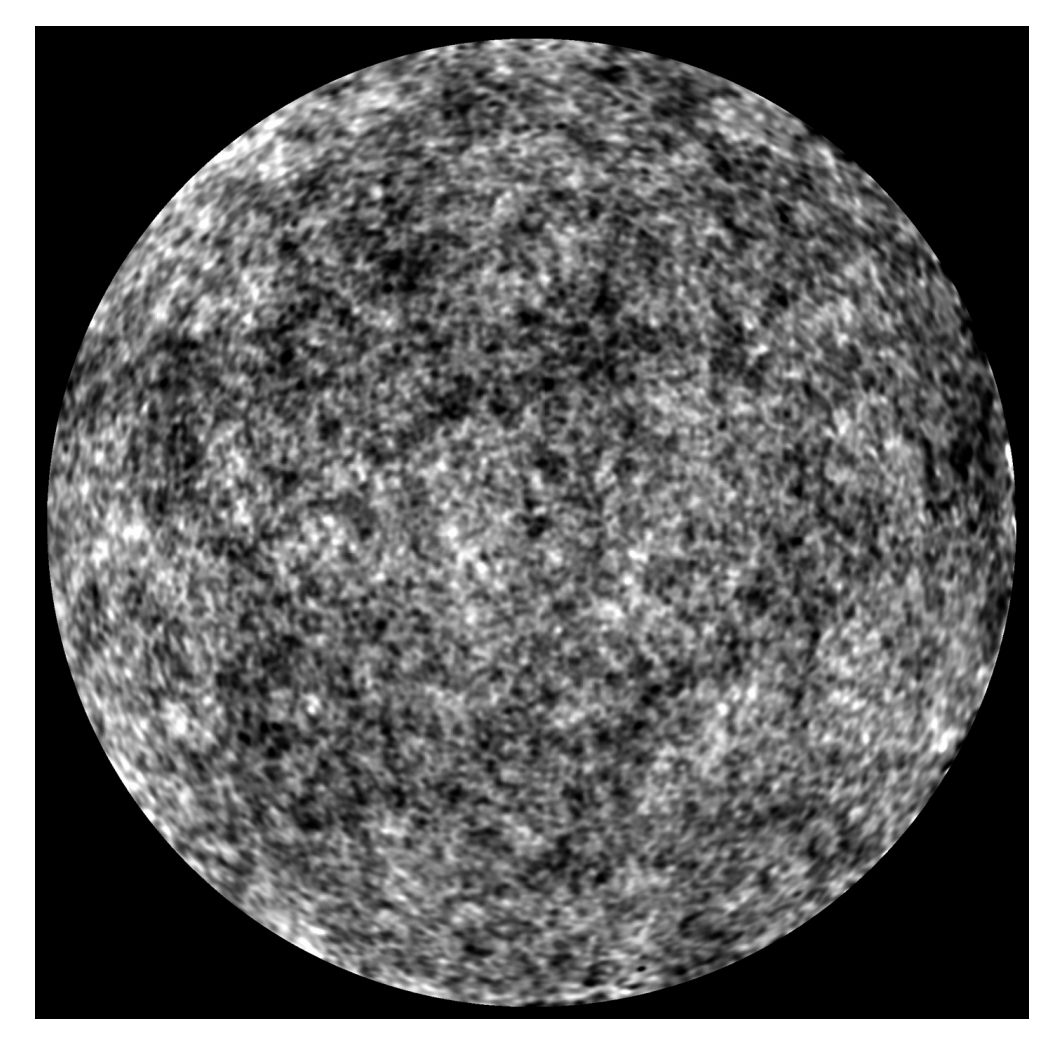


Figure 10.4 A half-sky (2π steradians) map of the temperature of the CMB sky. The typical relative fluctuations in the temperature, as coded by the gray scale (white is hot, black is cold), are of order 10^{-5} . Note the characteristic sizes of the hot and cold spots, \approx 0.4°. As described in the text, this size provides a "standard ruler" with which the geometry of space can be measured. Foreground microwave emission from the Milky Way has been subtracted from the image, as well as the CMB "dipole" anisotropy due to the motion of the Local Group relative to the comoving cosmological frame. Photo credit: NASA and the WMAP Science Team.

The speed of sound is then

$$c_{\rm s} = \sqrt{\frac{dP}{d\rho}} = \frac{c}{\sqrt{3}}.\tag{10.28}$$

The mass density inhomogeneities have a spatial spectrum with power spread continuously among all Fourier components, i.e., they have no single physical scale. (The particular shape of the Fourier spectrum is, as noted above, a prediction of inflationary theories.) The gravitational potential of the inhomogeneities attracts the baryon–photon fluid, which is compressed in the denser regions and more tenuous in the underdense regions. However,

the pressure of the fluid opposes the compression, and causes an expansion that stops only after the density has "overshot" the equilibrium density and the gas in the originally overdense region has become underdense. Thus, periodic expansion and contraction of the various fluid regions ensues. This means that "standing" sound waves of all wavelengths represented in the spatial Fourier spectrum of the density inhomogeneities are formed in the photon–baryon gas. 6 Their periods τ and wavelengths λ are related by

$$\tau = \frac{\lambda}{c_{\rm s}}.\tag{10.29}$$

When the Universe emerges from the inflationary era, at an age of a small fraction of a second, these **acoustic oscillations** are stationary and therefore they begin everywhere **in phase**. Consider now an overdense or underdense region. One of the Fourier modes that composes the region, and the fluid oscillations that it produces, has a wavelength that corresponds to a half-period of $t_{\rm rec}$,

$$\lambda = 2c_{\rm s}t_{\rm rec} = \frac{2ct_{\rm rec}}{\sqrt{3}},\tag{10.30}$$

where $t_{\rm rec}$ is the cosmic time when recombination occurs. At $t_{\rm rec}$, the baryon–photon fluid in this particular mode will have executed one-half of a full density oscillation, and will have just reached its maximal rarefaction or compression, where it will be colder or hotter, respectively, than the mean. At that time, however, the baryons and photons decouple, and the imprint of the cool (rarified) and hot (compressed) regions of the mode is frozen onto the CMB radiation field, and appears in the form of spots on the CMB sky with temperatures that are lower or higher than the mean. Similarly, higher modes that have had just enough time, between t=0 and $t=t_{\rm rec}$, to undergo one full compression and one full rarefaction, or two compressions and a rarefaction, etc., will also be at their hottest or coldest at time $t_{\rm rec}$. The CMB sky is therefore expected to display spots having particular sizes. Stated differently, the fluctuation power spectrum of the CMB sky should have discrete peaks at these favored spatial scales.

In reality, the picture is complicated by the fact that several processes, other than adiabatic compression, affect the gas temperature observed from each point. However, all these effects can be calculated accurately, and a prediction of the power spectrum can be made for a particular cosmological model. It turns out that measurement of the angular scales at the positions of the **acoustic peaks** in the power spectrum, and their relative heights, can determine most of the parameters describing a cosmological model. Let us see how this works for one example—the angular scale of the first acoustic peak as a measure of the global curvature of space.

As seen in Eq. 10.30, the physical scale of the first acoustic peak is the *sound-crossing horizon* at the time of recombination. It therefore provides an excellent "standard ruler" at

⁶ The waves that are formed are not, strictly speaking, standing waves, since they do not obey boundary conditions. They do resemble standing waves in the sense that a given Fourier component varies in phase at all locations. However, the superposition of all these waves is not a standing wave pattern, and does not have fixed nodes.

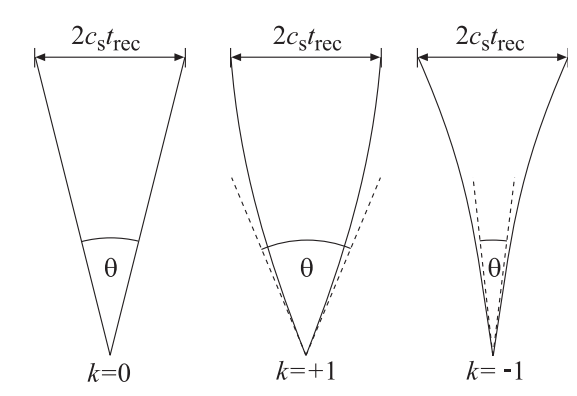


Figure 10.5 The angular diameter of the sound-crossing horizon (measurable from the size of the hot and cold spots in temperature anisotropy maps of the microwave sky), as it appears to observers in different space geometries. In a k=0 universe ("flat" space), the spots subtend on the sky an angle θ given by Euclidean geometry. In a k=+1 Universe, the angles of a triangle with sides along geodesics sum to >180°. Since light follows a geodesic path, the converging light rays from the two sides of a CMB "spot" will bend, as shown, along their path, and θ will appear larger than in the k=0 case. For negative space curvature, the angles in the triangle sum to <180°, and θ is smaller than in the flat case.

a known distance. The angle subtended on the sky by this standard ruler (i.e., the angle of the first peak) can be predicted for every geometry (i.e., curvature) of space. Comparison to the observed angle thus reveals directly what that geometry is (see Fig. 10.5).

Consider, for example, a flat (k = 0) cosmology with no cosmological constant. We wish to calculate the angular size on the sky, as it appears today, of a region of physical size (Eq. 10.30)

$$D_{\rm s} = \frac{2ct_{\rm rec}}{\sqrt{3}} = \frac{2 \times 380,000 \,\text{ly}}{\sqrt{3}} = 130 \,\text{kpc},$$
 (10.31)

from which light was emitted at time $t_{\rm rec}$. Between recombination and the present time, the Universal expansion is matter dominated, with $R \propto t^{2/3}$ for this model, i.e.,

$$\frac{R}{R_0} = \left(\frac{t}{t_0}\right)^{2/3} = \frac{1}{1+z},\tag{10.32}$$

and hence we can also write D_s as

$$D_{\rm s} = \frac{2ct_0}{\sqrt{3}} (1 + z_{\rm rec})^{-3/2}.$$
 (10.33)

The angle subtended by the region equals its size, divided by its distance to us *at the time of emission* (since that is when the angle between rays emanating from two sides of the region was set). As we are concerned with observed angles, the type of distance we are interested in is the distance that, when squared and multiplied by 4π , will give the area of the sphere centered on us and passing through the said region. If the comoving radial coordinate

of the surface of last scattering is r, the required distance is *currently* just $r \times R_0$, and is called the **proper-motion distance**. (For k = 0, the proper distance and the proper-motion distance are the same, as can be seen from Eq. 9.10.) The proper-motion distance can again be found by solving for the null geodesic in the FLRW metric (see Eq. 10.2),

$$\int_{t_{\text{rec}}}^{t_0} \frac{c \, dt}{R(t)} = \int_0^r \frac{dr}{\sqrt{1 - kr^2}}.$$
 (10.34)

Setting k = 0, and substituting

$$R(t) = R_0 \left(\frac{t}{t_0}\right)^{2/3},\tag{10.35}$$

we integrate and find

$$rR_0 = 3ct_0 \left[1 - \left(\frac{t_{\text{rec}}}{t_0} \right)^{1/3} \right] = 3ct_0 [1 - (1 + z_{\text{rec}})^{-1/2}].$$
 (10.36)

However, at the time of emission, the scale factor of the Universe was 1 + z times smaller. The so-called **angular-diameter distance** to the last scattering surface is therefore

$$D_A = \frac{rR_0}{1+z} = 3ct_0[(1+z_{\rm rec})^{-1} - (1+z_{\rm rec})^{-3/2}]. \tag{10.37}$$

The angular size of the sound-crossing horizon at the recombination era in a k = 0 cosmology is thus expected to be

$$\theta = \frac{D_{\rm s}}{D_{\rm A}} = \frac{2ct_0(1+z_{\rm rec})^{-3/2}}{3\sqrt{3}ct_0[(1+z_{\rm rec})^{-1} - (1+z_{\rm rec})^{-3/2}]}$$

$$= \frac{2}{3\sqrt{3}[(1+z_{\rm rec})^{1/2} - 1]}.$$
(10.38)

Since recombination occurs at $T_{\rm rec}\approx 3000$ K, and the current CMB temperature is 2.7 K, $z_{\rm rec}\approx 1100$, and

$$\theta \approx 0.012 \text{ radian} = 0.7^{\circ}. \tag{10.39}$$

For this particular cosmological model (k=0, $\Omega_{\Lambda}=0$), this will be the angular scale of the first acoustic peak in the Fourier spectrum of the CMB fluctuations. The hot and cold "spots" in CMB sky maps will correspond to half a wavelength, i.e., will have half this angular size, or somewhat smaller than the diameter of the full Moon (half a degree). In a negatively curved geometry, where the angles of a triangle add up to less than 180°, the angle subtended by the standard ruler of length $2c_{\rm s}t_{\rm rec}$ will be smaller than in a flat geometry. In a positively curved Universe, this angle will appear larger than in the flat case.

Measurements of the CMB fluctuation power spectrum provide spectacular confirmation of the expected acoustic peaks (see Fig. 10.6). When compared to more sophisticated

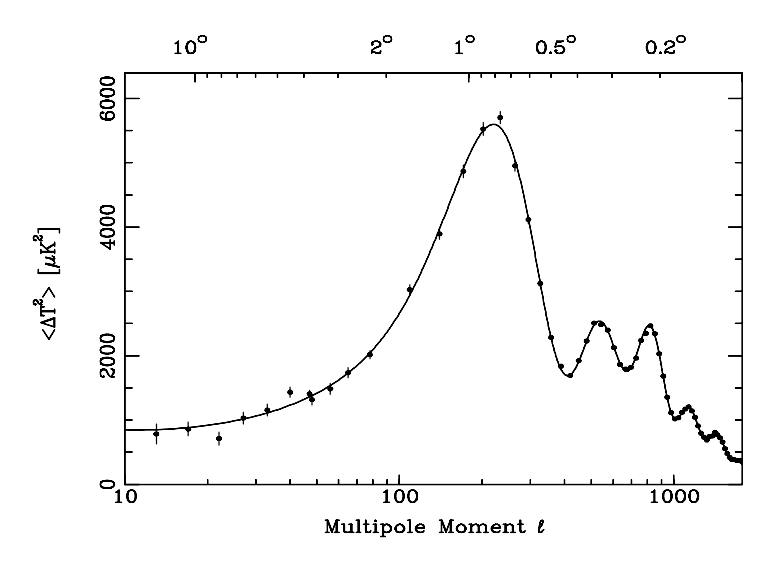


Figure 10.6 Observed angular power spectrum of temperature fluctuations in the CMB. The top axis shows the angular scales corresponding to the spherical harmonic multipoles on the bottom axis. The curve is based on a detailed calculation of the fluctuation spectrum using values for the various cosmological parameters that give the best fit to the data. Note the clear detection of acoustic peaks, with the first peak on a scale $\theta \approx 0.8^{\circ}$, indicating a flat space geometry. Data credits: WMAP and *Planck* collaborations.

calculations that account for all the known effects that can influence the temperature anisotropies, the location of the first peak indicates a nearly flat space geometry, with

$$\Omega_m + \Omega_{\Lambda} = 1.01 \pm 0.01. \tag{10.40}$$

Note that a region with the diameter of the sound-crossing horizon has, between recombination and the present, expanded by $1+z_{\rm rec}=1100$, and hence encompasses today (i.e., has a *comoving diameter*) 130 kpc \times 1100 = 150 Mpc. Thus, the CMB hot and cold spots correspond to regions that, today, are quite large.

Among a number of other cosmological parameters that are determined by analysis of the observed CMB anisotropy power spectrum is

$$\Omega_m \approx 0.3,$$
 (10.41)

which together with Eq. 10.40 confirms the result found from the Hubble diagram of type-Ia supernovae, that the dynamics of the Universe are currently dominated by a cosmological constant with

$$\Omega_{\Lambda} \approx 0.7.$$
 (10.42)

If one assumes that the Universe is exactly flat, then the CMB results also give a precise age of the Universe,

$$t_0 = 13.7 \pm 0.2 \,\text{Gyr},$$
 (10.43)

and a density in baryons,

$$\Omega_{\rm B} = 0.044 \pm 0.004. \tag{10.44}$$

The mere existence of acoustic peaks in the power spectrum means that density perturbations existed long before the time of recombination, i.e., they were *primordial*, and that they had wavelengths much longer than the horizon size at the time they were set up. Inflation is the only theory that currently predicts, based on causal physics, the existence of primordial, *superhorizon-size* perturbations. The observation of the acoustic peaks can therefore be considered as another successful prediction of inflation.

The large density inhomogeneities we see today—stars, galaxies, and clusters—formed from the growth of the initial small fluctuations, the traces of which are observed in the CMB. The gravitational pull of small density enhancements attracted additional mass, at the expense of neighboring underdense regions. The growing clumps of dense matter merged with other clumps to form larger clumps. This growth of structure by means of gravitational instability operated at first only on the nonbaryonic dark-matter fluctuations, but not the baryons, which were supported against gravitational collapse by radiation pressure. Once the expansion of the Universe became matter dominated, the dark-matter density perturbations could begin to grow at a significant rate. Finally, after recombination, the baryons became decoupled from the photons and their supporting radiation pressure, and the perturbations in the baryon density field could also begin to grow. The details and specific path according to which structure formation proceeds is still the subject of active research. Nevertheless, it is clear that, once the first massive stars formed (ending the period sometimes called the Dark Ages), they reionized most of the gas in the Universe. Based again on analysis of the CMB, current evidence is that this occurred during some redshift in the range between \sim 8 and 14, when the Universe was 300-600 Myr old.

By this time, the mean matter density was low enough that the newly liberated electrons were a negligible source of opacity, and hence the Universe remained transparent (see Problem 2). Direct evidence that most of the gas in the Universe is, at $z \sim 6$ and below, almost completely ionized, comes from the fact that objects at those redshifts are visible at UV wavelengths shorter than Lyman- α ; even a tiny number of neutral hydrogen atoms along the line of sight would suffice to completely absorb such UV radiation, due to the very large cross section for absorption from the ground state of hydrogen (often called resonant absorption). Most of the gas in the intergalactic medium (which is the main current repository of baryons) remains in a low-density, hot, ionized phase. The density of this gas is low enough that the recombination time is longer than the age of the Universe, and hence the atoms will never recombine.

10.4 Baryon Acoustic Oscillations

In section 10.3, we saw that the sound waves in the baryon–photon fluid, at the time of recombination, imprint anisotropies on the CMB sky on specific scales, producing the

acoustic peaks in the temperature fluctuation power spectrum. As we saw in Eq. 10.31, the first acoustic peak corresponds to a wavelength with a physical size equal to the diameter of the sound-crossing horizon,

$$D_{\rm s} = \frac{2ct_{\rm rec}}{\sqrt{3}} = 130 \,\mathrm{kpc},$$

providing a standard ruler at $z_{\rm rec}=1100$, with which the curvature of the Universe has been measured. This scale can serve as a standard ruler also at lower redshifts and later times, through the detection of **baryon acoustic oscillations**, as follows.

The overdensities in the matter-density field are preferred locations for the growth of perturbations, via gravitational instability (see above), into the structures that eventually become stars, galaxies, and galaxy clusters. Because there is often one wavelength D_s between two density enhancements in the CMB (that oftenness is the meaning of the peak in the power spectrum), at any redshift z there will be a favored separation, $D_s(1 + z_{rec})/(1 + z)$, imprinted on the distribution of distances between any two galaxies, or between any structures that trace the density field. As already noted in section 10.3, the sound-horizon diameter has a comoving (i.e., now, at z = 0) size of 150 Mpc.

At a given redshift range *z*, the *observed* separation between galaxies, in terms of angular separation on the sky and line-of-sight separation in redshift, will depend on the angular-diameter distance and on the proper distance, respectively. As with the case of type-Ia supernovae and their luminosity distances (section 10.1), the distance–redshift relations depend on the cosmological parameters, and thus the observed separations can provide a measurement of the cosmology. One way to quantify the distribution of distances between galaxies (or other objects), and to detect and measure the baryon acoustic oscillation scale, is by means of the *two-point correlation function*,

$$\xi(s) \equiv \frac{N_{\mathrm{obs}}(s)}{N_{\mathrm{ran}}(s)} - 1,$$

where $N_{\rm obs}(s)$ is the observed number of pairs of galaxies with separation s, and $N_{\rm ran}(s)$ is the number of such pairs expected at random from a uniformly distributed population, i.e., a population without any clustering. (In practice, one counts the numbers of galaxies with separations that are within a bin Δs around s.) If there is no clustering at a separation s, so $N_{\rm obs}(s) = N_{\rm ran}(s)$, then $\xi(s) = 0$. If galaxies completely avoid a certain separation s, $\xi(s)$ can be as low as -1 (the galaxies are anticorrelated at that separation). The correlation $\xi(s)$ can be arbitrarily high for strong clustering at some scale. Figure 10.7 shows the two-point correlation function measured for a sample of one million galaxies in the redshift range 0.2 < z < 0.7. The baryon acoustic oscillation scale, i.e., an enhanced tendency of galaxies to have a comoving separation of $s \approx 150$ Mpc, is apparent. The distance–redshift relation that gives this standard-ruler scale indicates the same values for the cosmological parameters as found using type-Ia supernovae and CMB anisotropies, i.e., k=0, $\Omega_m \approx 0.3$, and $\Omega_\Lambda \approx 0.7$.

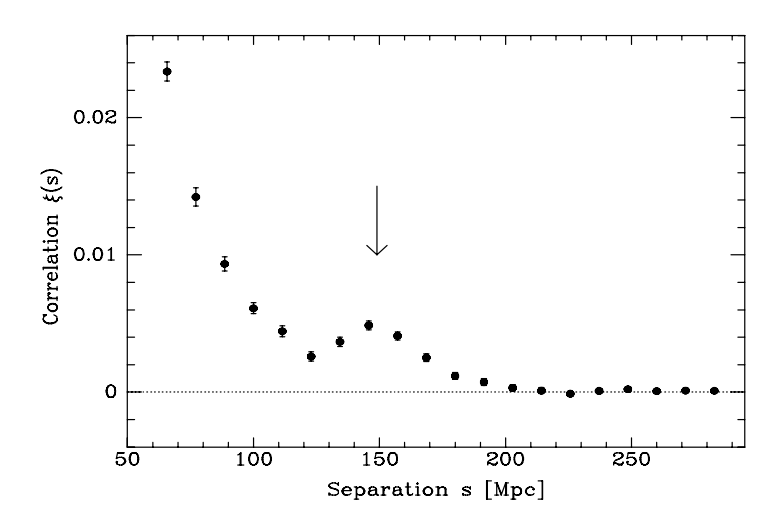


Figure 10.7 Two-point correlation function, $\xi(s)$, as a function of separation, for a million galaxies at 0.2 < z < 0.7. The acoustic peak at a comoving separation $s \approx 150$ Mpc is marked, and corresponds to the present-day size of the recombination-era sound-horizon diameter. As with the Hubble diagram of type-Ia supernovae (Fig. 10.2), the observed dependences on redshift of the angular diameter and proper distances to this standard ruler, for galaxy samples at various redshifts, constrain the cosmological parameters. Data credit: L. Anderson et al. 2014, *Mon. Not. Royal Astron. Soc.*, 441, 24.

10.5 Nucleosynthesis of the Light Elements

Looking back in time to even earlier epochs than those discussed so far, the temperature of the Universe must have been high enough that electrons, protons, positrons, and neutrons were in thermodynamical equilibrium. Since the rest-mass energy difference between a neutron and a proton is

$$(m_n - m_p)c^2 = 1.3 \text{ MeV},$$
 (10.45)

at a time $t \ll 1$ s, when the temperature was $T \gg 1$ MeV (10¹⁰ K), the reactions

$$e^- + p + 0.8 \text{ MeV} \rightleftharpoons \nu_e + n \tag{10.46}$$

and

$$\bar{\nu}_e + p + 1.8 \text{ MeV} \rightleftharpoons e^+ + n$$
 (10.47)

could easily proceed in both directions. The ratio between neutrons and protons as a function of temperature can be obtained from statistical mechanics considerations via the **Saha equation**. For the case at hand, it takes the form

© Copyright, Princeton University Press. No part of this book may be distributed, posted, or reproduced in any form by digital or mechanical means without prior written permission of the publisher.

264 | Chapter 10

$$\frac{N_n}{N_p} = \left(\frac{m_n}{m_p}\right)^{3/2} \exp\left[-\frac{(m_n - m_p)c^2}{kT}\right]. \tag{10.48}$$

When $T\gg 1$ MeV, the ratio is obviously very close to 1. As the temperature decreases, the ratio also decreases, and protons outnumber the heavier neutrons. This decrease in the ratio could continue indefinitely, but when T<0.8 MeV, the mean time for the reaction 10.46 becomes longer than the age of the Universe at that epoch, t=2 s. The reaction time can be calculated from knowledge of the densities of the different particles, the temperature, and the cross section, as outlined for stellar nuclear reactions in Eqs. 3.123–3.127. The long reaction timescale means that the neutrons and protons, which are converted from one to the other via this reaction are no longer in thermodynamic equilibrium. This time is called **neutron freezeout**, since neutrons can no longer be created. The neutron-to-proton ratio therefore "freezes" at a value of exp (-1.3/0.8)=0.20. In the following few minutes, most of the neutrons become integrated into helium nuclei. This occurs through the reactions

$$n + p \to d + \gamma, \tag{10.49}$$

$$p + d \rightarrow^{3} \text{He} + \gamma, \tag{10.50}$$

$$d + d \rightarrow^{3} \text{He} + n, \tag{10.51}$$

$$n + {}^{3}\text{He} \rightarrow {}^{4}\text{He} + \gamma, \tag{10.52}$$

$$d + {}^{3}\text{He} \rightarrow {}^{4}\text{He} + p.$$
 (10.53)

Some of the neutrons undergo beta decay into a proton and an electron before making it into a helium nucleus (the mean lifetime of a free neutron is about 15 min), and a small fraction is integrated into other elements. Numerical computation of the results of all the parallel nuclear reactions that occur as the Universe expands, and as the density and the temperature decrease, shows that, in the end, the ratio between neutrons inside ⁴He and protons is about 1/7. Thus, for every 2 neutrons there are 14 protons. Since every ⁴He nucleus has 2 neutrons and 2 protons, there are 12 free protons for every ⁴He nucleus, or the ratio of helium to hydrogen atoms is 1/12. The mass fraction of ⁴He will then be

$$Y_4 = \frac{4N(^4\text{He})}{N(\text{H}) + 4N(^4\text{He})} = \frac{4 \times \frac{1}{12}}{1 + 4 \times \frac{1}{12}} = \frac{1}{4}.$$
 (10.54)

A central prediction of Big Bang cosmology is therefore that a quarter of the mass in baryons was synthesized into helium in the first few minutes.

Measurements of helium abundance in many different astronomical settings (stars, H II regions, planetary nebulae) indeed reveal a helium mass abundance that is consistent with this prediction. This large amount of helium could not plausibly have been produced in stars. On the other hand, the fact that the helium abundance is nowhere observed to be lower than $\approx\!0.25$ is evidence for the unavoidability of primordial helium synthesis, at this level, among all baryons during the first few minutes.

⁷ At about the same time, neutrinos also *decouple* (i.e., cease to be in thermal equilibrium with the rest of the matter and the radiation), and the cosmic neutrino background is formed; see Problem 9.

Table 10.1 History and Parameters of the Universe

Curvature: $\Omega_m + \Omega_{\Lambda} = 1.01 \pm 0.01$ Mass density: $\Omega_{m,0} \approx 0.3$, consisting of

 $\Omega_{B,0}=0.044\pm0.004$ in baryons, and

 $\Omega_{DM,0}\approx 0.25$ in dark matter

Dark energy: $\Omega_{\Lambda} \approx 0.7$

Time	Redshift z	Temperature $T(K)$	Event
~10 ⁻³⁴ s	~10 ²⁷	~10 ²⁷	Inflation ends, $\Omega_m + \Omega_\Lambda \to 1$, causally connected regions have expanded exponentially, initial fluctuation spectrum determined.
2 s	4×10^9	10^{10}	Neutron freezeout, no more neutrons formed.
3 min	4 × 10 ⁸	10 ⁹	Primordial nucleosynthesis over—light element abundances set.
65,000 yr	3500	104	Radiation domination \to mass domination, $R \sim t^{1/2} \to R \sim t^{2/3}$, dark-matter structures start growing at a significant rate.
380,000 yr	1100	3000	Hydrogen atoms recombine, matter and radiation decouple, Universe becomes transparent to radiation of wavelengths longer than Ly α , CMB fluctuation pattern frozen in space, baryon perturbations start growing.
$\sim 10^8 - 10^9 \text{ yr}$	~6–20	~20–60	First stars form and reionize the Universe, ending the Dark Ages. The Universe becomes transparent also to radiation with wavelengths shorter than $Ly\alpha$.
∼6 Gyr	~1	~5	Transition from deceleration to acceleration under the influence of dark energy.
14 Gyr	0	2.725 ± 0.002	Today.

Apart from ⁴He, trace amounts of the following elements are produced during the first minutes: deuterium (10^{-5}), ³He (10^{-5}), ⁷Li (10^{-9}), ⁷Be (10^{-9}), and almost nothing else. The precise abundances of these elements depend on the baryon density, n_B , at the time of nucleosynthesis. As we have seen (Eqs. 9.40, 10.13), the radiation energy density declines as R^{-4} , but the temperature appearing in the Planck spectrum also declines as $T \propto 1/R$, both before and after recombination. Since the energy of the photons scales with kT, the photon **number** density declines as R^{-3} . Because baryons are conserved, their density also declines as R^{-3} when the Universe expands, and therefore the baryon-to-photon ratio

© Copyright, Princeton University Press. No part of this book may be distributed, posted, or reproduced in any form by digital or mechanical means without prior written permission of the publisher.

266 | Chapter 10

(Eq. 10.25), $\eta \approx 5 \times 10^{-10}$, does not change with time. Since we know the CMB photon density today, n_{γ} , measurements of the abundances of the light elements in astronomical systems that are believed to be pristine, i.e., that have undergone minimal additional processing in stars (which can also produce or destroy these elements) lead to an estimate of the baryon density today. In units of the critical closure density, $\rho_{\rm c}$,

$$\Omega_{\rm B} = \frac{n_B m_p}{\rho_{\rm c}} = \frac{\eta \ n_\gamma m_p}{\rho_{\rm c}}.\tag{10.55}$$

The baryon density based on these measurements is

$$0.01 < \Omega_{\rm B} < 0.05.$$
 (10.56)

As already mentioned, a completely independent estimate of Ω_B comes from analyzing the fluctuation spectrum of CMB anisotropies. The relative amplitudes of the acoustic peaks in the spectrum depend on the baryon density and hence constrain it to

$$\Omega_{\rm B} = 0.044 \pm 0.004,\tag{10.57}$$

in excellent agreement with the value based on element abundances. Note that both of these measurements tell us that, even though the mass density of the Universe is a good fraction of the closure value ($\Omega_m \approx 0.3$), only about a tenth of this mass is in baryons, while the rest must be in a dark matter component of unknown nature. Furthermore, less than 1/10 of the baryons are in stars inside galaxies. The bulk of the baryons are apparently in a tenuous, hot, and ionized intergalactic gas—the large reservoir of raw material out of which galaxies formed. A small fraction of this gas is neutral, and can be observed by the absorption it produces in the spectra of distant quasars. This is discussed briefly in section 10.6.

Table 10.1 summarizes the current view of the cosmological parameters and the history of the Universe.

10.6 Quasars and Other Distant Sources as Cosmological Probes

Quasars, which we discussed in chapter 7.3, are supermassive black holes accreting at rates that produce near-Eddington luminosities of 10^1 – 10^4L_* . Their large luminosities make quasars easily visible to large cosmological distances, and allow probing the assembly and accretion history of the central black holes of galaxies. As noted in chapter 7, luminous quasars are rare objects at present, and apparently most central black holes in nearby galaxies are accreting at low or moderate rates, compared to the rates that would produce a luminosity of $L_{\rm E}$. However, quasars were much more common in the past, and their comoving space density reached a peak at an epoch corresponding to redshift $z \sim 2$ (i.e., about 10 Gyr ago). There is likely a connection between the growth and development of galaxies and of their central black holes, and quasar evolution may hold clues to deciphering this connection (see Problem 11). The most distant quasars currently known are at redshifts up to z = 7, and are therefore observed less than 1 Gyr after the Big Bang. Models of structure formation suggest that the first galaxies began to assemble at about that time.

Since quasars are so luminous, they are also useful cosmological tools, in that they can serve as bright and distant sources of light for studying the contents of the Universe



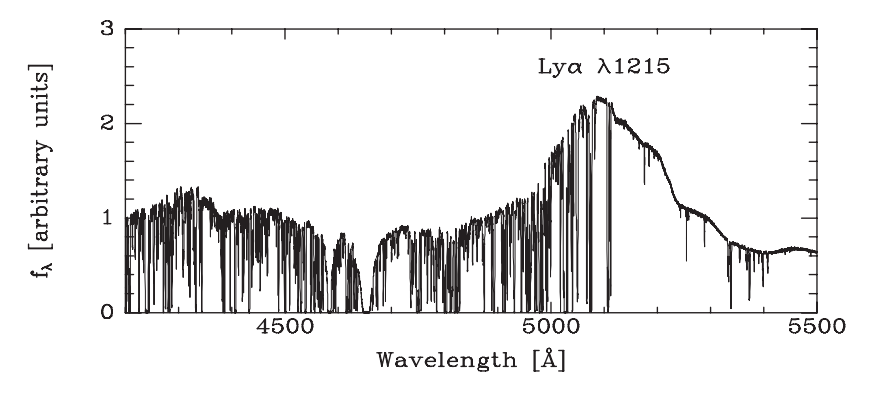


Figure 10.8 A high-resolution spectrum of a quasar at redshift z = 3.18, with the Lyman- α emission line redshifted to 5080 Å. Note the *Lyman-α forest* of absorption lines starting from the peak of the emission line, and continuing in the blue (left) direction. These lines are due to Lyman- α absorption by neutral hydrogen atoms in gas clouds that are along the line of sight to the quasar, and hence at lower redshifts than the quasar. The few absorption lines to the red of the Lyman- α emission-line peak are due to heavier elements and are associated with the system that produces the strong damped Lyman- α absorption observed at \approx 4650 Å. Data credit: W. Sargent and L. Lu, based on observations with the HIRES spectrograph at the W. M. Keck Observatory.

between the quasars and us. One such application is the study of quasar absorption lines. The light from all distant quasars is seen to be partially absorbed by numerous clouds of gas along the line of sight. A small fraction ($\sim 10^{-4}$) of the hydrogen in these clouds is neutral, and is manifest as a "forest" of redshifted absorption lines (mostly Lyman- α) in the spectrum of each quasar (see Fig. 10.8). Each absorption line is at the wavelength of Lyman- α redshifted according to the distance of the particular absorbing cloud. The absorption lines are therefore distributed in wavelength between the rest wavelength of Ly α at 1216 Å and the observed, redshifted Ly α wavelength of the quasar (say, (1+z)1216 Å = 3648 Å, for a z = 2 quasar).

Apart from the hydrogen Lyman- α lines, additional absorption lines are detected. Absorption lines produced by heavier elements in the same clouds allow estimating the "metallicities" of these clouds, and reveal very low element abundances, i.e., the gas in the clouds has undergone little enrichment by stellar processes. It is in such clouds that the abundance of primordial deuterium can be measured and compared to Big Bang nucleosynthesis predictions (see section 10.5). The Lyman- α clouds are one component (a relatively cool one, with $T \sim 10^4$ K) of the intergalactic medium. Most of the intergalactic gas, however, is apparently in a hotter $T \sim 10^5 - 10^6$ K, more tenuous component. Estimates of the total mass density of intergalactic gas find that the bulk of the baryons in the Universe is contained in this hot component, while less than about 10% of the baryons are in galaxies in the form of stars and cold gas.

Another application in which quasars serve as distant light sources for probing the intervening matter distribution is in cases where galaxies or galaxy clusters gravitationally

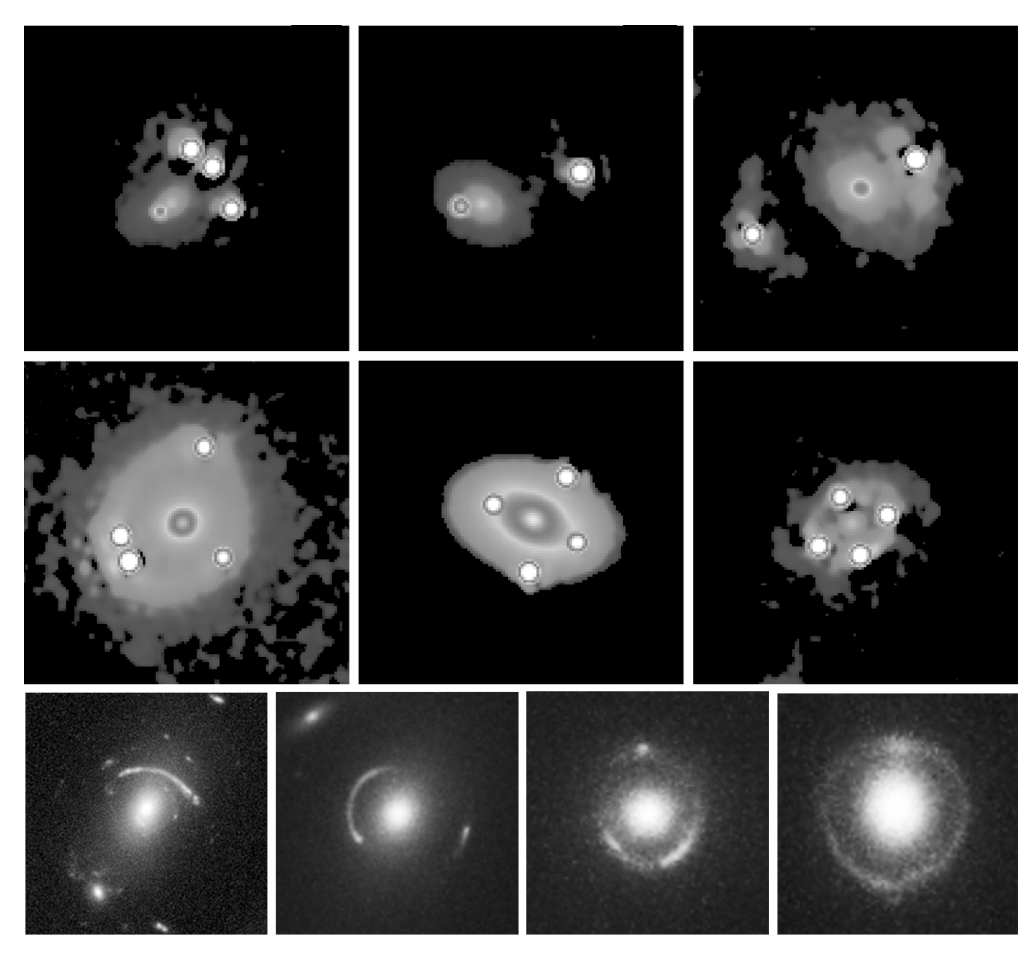


Figure 10.9 *Top two rows*: Examples of quasars that are gravitationally lensed into multiple images by intervening galaxies. In each case, the lens galaxy, at a redshift of $z\approx0.04$ –0.7, is the extended central object, and the two or four sources straddling it are the multiply lensed images of a background quasar, at $z\approx1.7$ –3.6. Panels are 5 arcseconds on a side. Some image processing has been applied, to permit seeing clearly both the bright, point-like, quasar images and the faint, extended lens galaxies. *Bottom row*: Examples of foreground galaxies that lens background galaxies into partial or full Einstein rings. In the cases shown, the foreground galaxies are at $z\approx0.2$ –0.4 and the background galaxies are at $z\approx0.5$ –1. Photo credits: The CASTLES gravitational lens database, C. Kochanek et al.; NASA, ESA, J. Blakeslee and H. Ford,; and NASA, ESA, A. Bolton, S. Burles, L. Koopmans, T. Treu, and L. Moustakas.

lens quasars that are projected behind them, splitting them into multiple images.⁸ Since the lensing objects in such cases are at cosmological distances (\sim 1 Gpc), and the lensing masses are of order $10^{11}M_{\odot}$, the Einstein angle (Eq. 6.16), which gives the characteristic angular scale of the split images, is of order 1 arcsecond, i.e., resolved by telescopes at most wavelength bands, from radio through X-rays (see Fig. 10.9). Modeling of individual systems can reveal the shapes and forms of the mass distributions, both the dark and the

⁸ Since galaxy mass distributions are generally not spherically symmetric, when they act as gravitational lenses they can split background sources into multiple images, rather than just deforming the sources into rings or splitting them into double images, as is the case for point masses and spherically symmetric masses.

luminous. The statistics of lensed quasars (e.g., measurement of the fraction of quasars that are multiply imaged by intervening galaxies) can provide information on the properties of the galaxy population and its evolution with cosmic time (see chapter 7, Problem 5). Not only quasars serve as background light sources for galaxy lenses—there are many known cases of galaxies that lens other galaxies that lie behind them (also shown in Fig. 10.9), and such systems can be used for the same applications.

In known systems in which a galaxy or a galaxy cluster operates as a powerful gravitational lens, one can turn the problem around and use the lens as a "natural telescope." Once the properties of the lens have been derived, based on the positions and relative magnifications of the lensed images of the bright background quasar or galaxy, one can search other regions of the lens that are then expected to produce high magnification for lensed images of additional background objects. This method of "searching under the magnifying glass" has been used to find and study galaxies with luminosities as low as $0.01L_*$ out to redshifts $z\sim 10$, aided by the natural magnification of galaxy clusters.

With these and other techniques, it is hoped that a detailed and consistent picture of cosmic history will eventually emerge. Such an understanding would include the nature of dark matter and dark energy, their interplay with baryons and with supermassive black holes in the formation of the first stars and galaxies, the element enrichment of the interstellar and the intergalactic medium by generations of evolved stars and supernovae, and the evolution of galaxies and their constituents, all the way to the world as we see it today.

Problems

- 1. In an accelerating or decelerating Universe, the redshift z of a particular source will slowly change over time t_0 , as measured by an observer.
 - a. Show that the rate of change is

$$\frac{dz}{dt_0} = H_0(1+z) - H(z),$$

where $H(z) \equiv \dot{R}_e/R_e$ is the Hubble parameter at the time of emission.

Hint: Differentiate the definition of redshift, $1 + z \equiv R_0/R_e$, with respect to t_0 . Use the chain rule to deal with expressions such as dR_e/dt_0 .

b. Show that, for a k=0 universe with no cosmological constant, $H(z)=H_0(1+z)^{3/2}$. For this model, and assuming $H_0=70\,\mathrm{km\,s^{-1}}$ Mpc⁻¹, evaluate the change in redshift over 10 years, for a source at z=1, and the corresponding change in "recession velocity."

Answers:
$$\Delta z = -5.9 \times 10^{-10}$$
, $\Delta v = -18$ cm s⁻¹.

2. At a redshift z = 1100, atoms were formed, the opacity of the Universe to radiation via electron scattering disappeared, and the cosmic microwave background was formed. Imagine a world in which atoms cannot form. Even though such a universe, by definition, will remain ionized forever, after enough time the density will decline sufficiently to

make the universe transparent nonetheless. Find the redshift at which this would have happened, for a k = 0 universe with no cosmological constant. Assume an all-hydrogen composition, $\Omega_B = 0.04$, and $H_0 = 70$ km s⁻¹ Mpc⁻¹. Note that this calculation is not so far-fetched. Following recombination to atoms at z = 1100, most of the gas in the Universe was reionized between z = 8 and z = 14 (probably by the first massive stars that formed), and has remained ionized to this day. Despite this fact, the opacity due to electron scattering is very low, and our view is virtually unhindered out to high redshifts. Hint: A "Universe transparent to electron scattering" can be defined in several ways. One definition is to require that the rate at which a photon is scattered by electrons, $n_e \sigma_T c$, is lower than the expansion rate of the Universe at that time, H (or, in other words, the time between two scatters is longer than the age of the Universe at that time). To follow this path (which is called decoupling between the photons and the hypothetical free electrons), express the electron density n_e at redshift z, by starting with the current baryon number density, $\Omega_B \rho_{cr,0}/m_p$, expressing $\rho_{cr,0}$ by means of H_0 , and increasing the density in the past as $(1 + z)^3$. Similarly, write H in terms of H_0 and (1+z) (recall that $1+z=R_0/R$, and in this cosmology, $R \propto t^{2/3}$ and $H \propto t^{-1}$). Show that decoupling would have occurred at

$$1 + z = \left(\frac{8\pi \, Gm_p}{3\Omega_{\rm B} H_0 \sigma_{\rm T} c}\right)^{2/3},$$

and calculate the value of this redshift. Alternatively, we can find the redshift of the "last scattering surface" from which a typical photon would have reached us without further scatters. The number of scatters on electrons that a photon undergoes as it travels from redshift z to redshift zero is

$$\int_0^{l(z)} n_e(z) \sigma_{\rm T} dl.$$

Express n_e , as above, in terms of Ω_B , H_0 , and 1+z, replace dl with c(dt/dz)dz, using again $R \propto t^{2/3}$ to write dt/dz in terms of H_0 and 1+z. Equate the integral to 1, perform the integration, show that the last scattering redshift would be

$$1+z=\left(\frac{4\pi\,Gm_p}{\Omega_{\rm B}H_0\sigma_{\rm T}c}\right)^{2/3},$$

and evaluate it.

Answers: z = 65; z = 85.

3. Show that the angular-diameter distance for a flat space (k = 0; Eq. 10.37) out to redshift z.

$$D_A = 3ct_0[(1+z)^{-1} - (1+z)^{-3/2}],$$

has a maximum with respect to redshift z, and find that redshift. The angular size on the sky of an object with physical size d is $\theta = d/D_A$. What is the implication of the maximum of D_A for the appearance of objects at redshifts beyond the one you found?

Note that this peculiar behavior is simply the result of light travel time out to different distances in an expanding universe; an object at high redshift may have been closer to us at the time of emission than an object of the same size at a lower redshift, despite the fact that the high-redshift object is currently more distant.

4. a. Consider the energy flux of photons from a source with bolometric luminosity L and with proper-motion distance rR_0 . The photons will be spread over an area $4\pi (rR_0)^2$. Explain why the observed energy flux will be

$$f = \frac{L}{4\pi (rR_0)^2 (1+z)^2}.$$

Hint: Consider the effects of redshift on the photon energy and cosmological time dilation on the photon arrival rate. This relation is used to define the *luminosity* distance, $D_L = rR_0(1+z)$.

- b. Find $D_L(z)$ for a k = 0 universe without a cosmological constant. Plot, for this world model, the Hubble diagram, i.e., the flux vs. z, from an object of constant luminosity.
- **5.** Show that in a Euclidean, nonexpanding, universe, the surface brightness of an object, i.e., its observed flux per unit solid angle (e.g., per arcsecond squared), does not change with distance. Then, show that in an expanding FLRW universe, the ratio between the luminosity distance (see Problem 4) and the angular-diameter distance to an object is always $(1+z)^2$. Use this to prove that, in the latter universe, surface brightness dims with increasing redshift as $(1+z)^{-4}$. This effect makes extended objects, such as galaxies, increasingly difficult to detect at high z.
- **6.** An object at proper-motion distance rR_0 splits into two halves. Each piece moves relative to the other, perpendicular to our line of sight, at a constant, nonrelativistic, velocity v. What is the angular rate of separation, or "proper motion" between the two objects (i.e., the change of angle per unit time)?

Hint: Recall that we are measuring an angle, and so require the angular-diameter distance, but we are also measuring a rate, which is affected by cosmological time dilation. You can now see why rR_0 is called the proper-motion distance.

7. Use the first Friedmann equation with a nonzero cosmological constant (Eq. 9.95) to show that, in a flat, matter-dominated Universe, the proper-motion distance is

$$rR_0 = \int \frac{c \, dz}{H_0 \sqrt{\Omega_{m,0} (1+z)^3 + \Omega_{\Lambda,0}}}.$$

Use a computer to evaluate this integral numerically with $\Omega_{m,0}=0.3$ and $\Omega_{\Lambda,0}=0.7$, for values of z between 0 and 2. Plot the Hubble diagram, i.e., flux vs. z, from an object of constant luminosity, in this case, and compare to the curve describing k=0, $\Omega_m=1$ (Problem 4). You can now see how the Hubble diagram of type-Ia supernovae can distinguish among cosmological models.

Hint: Set k=0 in Eq. 9.95, replace ρ by $\rho_0R_0^3/R^3$ (matter domination), divide both sides by H_0^2 , and substitute the dimensionless parameters $\Omega_{m,0}$ and $\Omega_{\Lambda,0}$. Change variables from R to z with the transformation $1+z=R_0/R$, and separate the variables z and t. Finally, use the FLRW metric for k=0: $c\,dt=R\,dr=R_0/(1+z)dr$, and hence $rR_0=\int (1+z)c\,dt$, to obtain the desired result.

- **8.** Emission lines of hydrogen H β ($n = 4 \rightarrow 2$, $\lambda_{rest} = 4861$ Å) are observed in the spectrum of a spiral galaxy at redshift z = 0.9. The galaxy disk is inclined by 45° to the line of sight.
 - a. The H β wavelength of lines from one side of the galaxy is shifted to the blue by 5 Å relative to the emission line from the center of the galaxy, and to the red by 5 Å on the other side. What is the galaxy's rotation speed?
 - b. Analysis of the emission from the active nucleus of the galaxy reveals a total redshift of z=1. If the additional redshift is gravitational, the result of the proximity of the emitting material to a black hole, find this proximity, in Schwarzschild radii.

Hint: Note that all redshift and blueshift effects are multiplicative, e.g., $(1 + z_{\text{total}}) = (1 + z_{\text{cosmological}})(1 + v \sin i/c)$, or $(1 + z_{\text{total}}) = (1 + z_{\text{cosmological}})(1 + z_{\text{gravitational}})$.

- c. Find the age of the Universe at z=0.9, assuming an expansion factor $R \propto t^{2/3}$, and a current age $t_0=14$ Gyr. What is the "lookback time" to the galaxy? Answers: 230 km s⁻¹; 11 r_s ; lookback time 8.5 Gyr.
- 9. At some point back in cosmic time, the Universe was dense enough to be opaque to neutrinos. Then, as the Universe expanded, the density decreased until neutrinos could stream freely. A cosmic neutrino background (which is undetected to date) must have formed when this decoupling between neutrinos and normal matter occurred, in analogy to the CMB that results from the electron-photon decoupling at the time of hydrogen recombination. Find the temperature at which neutrino decoupling occurred. Assume in your calculation that decoupling occurs during the radiation-dominated era, photons pose the main targets for the neutrinos, neutrino interactions have an energy-dependent cross section

$$\sigma_{\nu\gamma} = 10^{-43} \text{ cm}^2 \left(\frac{E_{\nu}}{1 \text{ MeV}}\right)^2,$$

and the neutrinos are relativistic. Use a k = 0, $\Omega_{\Lambda} = 0$ cosmology.

Hint: Proceed by the first method of Problem 2, i.e., by requiring $n\sigma v = H$. Represent the "target" density, n, by aT^4/kT , where a is the Stefan–Boltzmann (or "radiation") constant. Use $\sigma_{\nu\gamma}$ for the cross section σ , but approximating E_{ν} as kT. The velocity v equals c, because the neutrinos and the target particles are relativistic. To represent H, use the first Friedmann equation,

$$H^2 = \frac{8\pi G \rho_{\rm rad}}{3c^2},$$

with $\rho_{\rm rad} = aT^4$.

Answer: kT = 1 MeV.

- 10. It has been found recently that every galactic bulge harbors a central black hole with a mass \sim 0.001 of the bulge mass. The mean space density of bulges having $10^{10} M_{\odot}$ is about $10^{-2} \, \mathrm{Mpc^{-3}}$.
 - a. Find the mean density of mass in black holes, in units of M_{\odot} Mpc⁻³.
 - b. If all these black holes were shining at their Eddington luminosities, what would be the luminosity density, in units of L_{\odot} Mpc⁻³? How does this compare to the luminosity density from stars?
 - c. The observed luminosity density of quasars and active galaxies, averaged over cosmic time, is actually 100 times less than calculated in (b). If all central black holes have gone through an active phase, what does this imply for the total length of time that a black hole is "active"?
- 11. The most distant quasars currently known are at redshift $z \sim 6$, and have luminosities $L \sim 10^{47} \ {\rm erg \ s^{-1}}$.
 - a. Find a lower limit to the mass of the black hole powering such a quasar, by assuming it is radiating at the Eddington limit.
 - b. Find the age of the Universe at z=6, assuming an expansion $R \propto t^{2/3}$ and a current age $t_0=14$ Gyr.
 - c. Equate the Eddington luminosity $L_E(M)$ as a function of mass M to the luminosity of an accretion disk around a black hole with a mass-to-energy conversion efficiency of 0.06. This will give you a simple differential equation for M(t), describing the growth of a black hole. Solve the equation (be careful with units).
 - d. Suppose a black hole begins with a "seed" mass of $10M_{\odot}$ and shines at the Eddington luminosity continuously. How long will it take the black hole to reach the mass found in (a)? By comparing to the result of (b), what is the minimum redshift at which accretion must begin?

Answers: $\sim 10^9 M_{\odot}$; t(z=6)=740 Myr; $M=M_{\rm seed} \exp(t/\tau)$, with $\tau=26$ Myr; 480 Myr, z(t=260 Myr) = 13.